Quantum capacitance and density of states of graphene

2012 Phys. Scr. 2012 014009

(http://iopscience.iop.org/1402-4896/2012/T146/014009)

Phys. Scr. **T146** (2012) 014009 (5pp) doi:10.1088/0031-8949/2012/T146/014009

Quantum capacitance and density of states of graphene

S Dröscher[1], P Roulleau[1], F Molitor[1], P Studerus[1], C Stampfer[2], K Ensslin[1] and T Ihn[1]

[1] Solid State Physics Laboratory, ETH Zurich, 8093 Zurich, Switzerland
[2] JARA-FIT and II, Institute of Physics, RWTH Aachen, 52074 Aachen, Germany

E-mail: susanned@phys.ethz.ch

Received 18 April 2011
Accepted for publication 8 June 2011
Published 31 January 2012
Online at stacks.iop.org/PhysScr/T146/014009

Abstract
We report capacitance measurements in top-gated graphene sheets as a function of charge carrier density. A measurement method using an *LC*-circuit provides high sensitivity to small capacitance changes and hence allows the observation of the quantum part of the capacitance. The extracted density of states has a finite value of $1 \times 10^{17}\,\mathrm{m}^{-2}\,\mathrm{eV}^{-1}$ in the vicinity of the Dirac point, which is in contrast to the theoretical prediction for ideal graphene. We attribute this discrepancy to fluctuations of the electrostatic potential with a typical amplitude of 100 meV in our device.

PACS numbers: 81.05.ue, 72.80.Vp, 84.37.+q

(Some figures may appear in colour only in the online journal)

1. Introduction

The number of available electronic states at the Fermi level determines the transport characteristics of electronic devices. A solid understanding of the density of states is hence crucial for the interpretation of the electronic properties a given system exhibits. In two-dimensional (2D) electron gases in semiconductor heterostructures, experiments mapping the density of states directly via the quantum capacitance were conducted in the 1980s [1 (and references [6–12] therein), 2] and are today standard characterization tools for these structures. More recently, the energy level spectrum of carbon nanotubes was experimentally observed in measurements of the quantum capacitance [3].

An infinite single-layer graphene sheet is expected to show a linear density of states that vanishes at the charge neutrality point [4]. The experimental findings of conductance measurements, however, contrast this theoretical prediction by showing a minimum conductivity of the order of $4(e^2/h)$, which indicates a finite charge carrier density [5, 6]. Since the quantum term in the capacitance gives insight into the density of states, both theoretical [7, 8] and experimental [9–11] studies of the quantum capacitance have been carried out for graphene within the last few years. All measurements show a nonzero value of the density of states at the Dirac point, which is commonly interpreted as originating from potential fluctuations in the graphene sheet. Here, we discuss experiments on a top-gated single-layer graphene ribbon and analyse the data in a self-consistent manner not making any theoretical assumptions about the density of states.

2. Theoretical background

A classical plate capacitor consists of two well-conducting plates arranged in parallel to each other and separated by a dielectric layer of a certain thickness. Its capacitance can be calculated considering material and geometric parameters of the system. If the density of states on one of the plates is finite, however, adding a charge carrier costs kinetic energy due to the shift of the Fermi level. Since this required extra energy reduces the total capacitance of the system, the density of states is directly reflected in an additional capacitance term. As visualized in the cross-section in figure 1(a), a locally gated graphene device can be viewed as a plate capacitor, with one plate being the top-gate electrode and the other being the graphene sheet.

The total capacitance between the gate and the electron gas can be derived from the electrostatics describing the system [12–14]. A finite applied bias $-|e|V_{\mathrm{TG}}$ introduces a difference in the electrochemical potentials of the metal

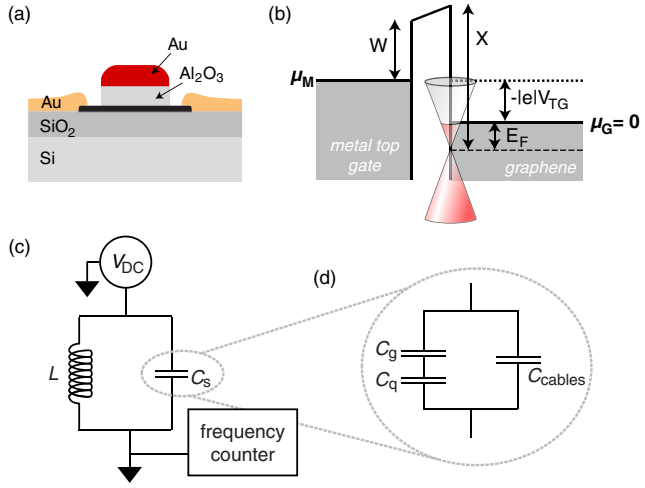

Figure 1. (a) Schematic cross-section of a top-gated graphene sample. The graphene flake (black) is contacted with gold electrodes (orange) and covered partly by an alumina/gold top-gate (grey/red). (b) Schematic diagram of the electrostatics of the structure showing the change in electrochemical potential between the top-gate electrode and the graphene sheet. (c) Circuit scheme of the measured system.

top-gate electrode, μ_M, and of the graphene, μ_G. As sketched in figure 1(b), it consists of the Fermi energy E_F in graphene, the electrostatic potential across the dielectric as obtained by solving Poisson's equation, and the two work functions χ and W of graphene and the metal, respectively. The effective potential difference is therefore given by

$$\mu_G - \mu_M = |e|V_{TG} = E_F + \frac{|e|^2 n_s}{\epsilon\epsilon_0} d + \text{const}, \qquad (1)$$

where n_s is the charge carrier density in the graphene layer, d is the thickness of the dielectric layer and the constant term includes the work function difference of the two materials, which can be neglected for the analysis provided that it is gate-voltage-independent. Differentiating equation (1) with respect to n_s gives an expression for the capacitance per unit area,

$$\frac{1}{C/A} = \frac{\mathrm{d}(|e|V_{TG})}{e^2 \mathrm{d}n_s} = \frac{\mathrm{d}E_F(n_s)}{e^2 \mathrm{d}n_s} + \frac{d}{\epsilon\epsilon_0}, \qquad (2)$$

where the second term on the right-hand side can be identified as the inverse of the geometric capacitance per unit area C_g/A. The other term has the dimensions of a capacitance and is inversely proportional to the density of states $\mathcal{D}(E_F) = \mathrm{d}n_s/\mathrm{d}E_F$. The quantity $e^2\mathcal{D}(E_F)$ is the so-called quantum capacitance per unit area C_q/A [12], which describes an effective decrease of the total sample capacitance. Since it is connected in series to C_g, the quantum capacitance will dominate the total capacitance if it takes values smaller than C_g.

3. Measurement setup

The temperature for all measurements was 1.7 K, achieved in a variable temperature insert ^{4}He cryostat. For basic characterization of the device, transport measurements using standard lock-in techniques were carried out in addition to quantum capacitance measurements. For the latter, the size of the expected signal was of the order of several fF and hence a high measurement resolution was required. Since frequencies can be measured with high accuracy, we used an *LC*-circuit and recorded changes in its resonance frequency f_{res}. Figure 1(c) shows the circuit model of our setup, with the oscillator consisting of an inductor ($L = 100\,\mu$H) placed at room temperature in parallel to the setup capacitance C. The main contribution to C comes from the wiring of the cryostat with a capacitance $C_{cables} \approx 340$ pF for the coaxial cables. In parallel to this, the series connection of C_g and C_q forms the sample capacitance C_s.

During the measurements, an oscillation amplitude of 20 mV was maintained in the resonator by an external drive. The resulting self-resonant frequencies were 850–900 kHz and the relative sensitivity for frequency changes was $\Delta f \approx 2.5 \times 10^{-7}$. Converted to capacitance changes, an accuracy of the order of 170 aF was achievable with this setup.

4. Sample fabrication

Standard mechanical exfoliation [15] of graphite flakes was used to obtain few-layer graphene on Si/SiO_2 substrate. To exclude stray capacitances from the back gate, the silicon substrate was undoped. Single-layer flakes were identified using an optical microscope, and subsequent atomic force microscopy (AFM) measurements as well as Raman spectroscopy [16, 17] were carried out to verify their single-layer nature. By electron beam lithography and subsequent evaporation of Cr/Au (2 nm/40 nm), electrical contacts were defined. The graphene sheets were structured by reactive ion etching and a patterned top-gate was deposited after a third electron beam lithography step. As a dielectric for the top-gate, we used Al_2O_3, which was obtained in cycles of depositing 1 nm of aluminum followed by a 3 min period of increased oxygen pressure in the deposition chamber leading to the complete oxidation of the thin Al film. The resulting oxide thickness of four such cycles is approximately 12 nm. Deposition of Ti/Au (5 nm/50 nm) in the same evaporation chamber formed the top-gate electrode. Figure 2(a) displays an AFM image of the device measured for this work.

5. Results and discussion

Figure 2(b) shows a two-terminal transport measurement taken with a current bias of 1 nA. The Dirac point is visible as a resistance maximum and only slightly shifted away from zero top-gate voltage. Since we do not know the precise thickness and the dielectric constant of the aluminum oxide, we can only estimate the geometric capacitance of the top-gate to be $C_g \approx 6\,\mathrm{fF}\,\mu\mathrm{m}^{-2}$. Using this estimate, a mobility of 2000–3000 $\mathrm{cm}^2\,\mathrm{V}\,\mathrm{s}^{-1}$ is extracted for the device.

The change in resonance frequency f_{res} as a function of applied top-gate voltage V_{TG} is displayed in figure 3(a). A maximum is observed close to zero gate voltage, which coincides with the maximum in the transport curve (figure 2(b)) and therefore marks the Dirac point. At high charge carrier densities, the resonance frequency reaches a constant value, indicating the dominant influence of the cable capacitance. We are interested in the relative change of f_{res}

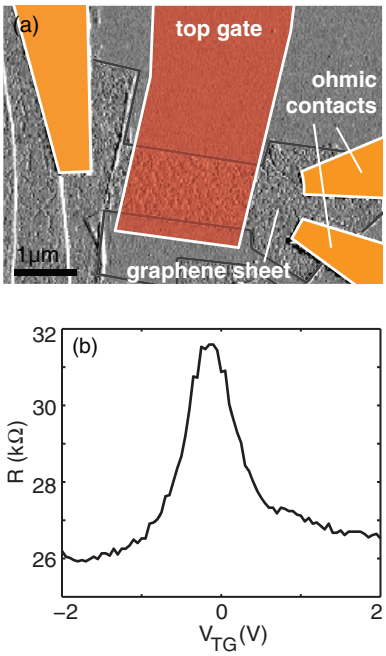

Figure 2. (a) Atomic force microscope image of the device studied here. The electrodes are coloured corresponding to the scheme in figure 1(a). (b) Two-point resistance obtained in transport measurements.

and therefore define the magnitude $\delta_m \equiv \Delta f(V_{TG})/f_0$, with f_0 being the voltage-independent background frequency (see the right scale in figure 3(a)).

To determine the changes in quantum capacitance from the frequency measurement, the circuit diagram has to be considered. Far away from the Dirac point, we expect C_q to be too large to affect the total capacitance, which is hence given by $C_{cables} + C_g$ in this limit. The total capacitance of the equivalent circuit in figure 1(d) can be written as

$$C(V_{TG}) = C_{cables} + C_g - \left[C_g - \left(\frac{1}{C_g} + \frac{1}{C_q} \right)^{-1} \right], \quad (3)$$

where the term outside the square brackets is constant at all top-gate voltages and only the term inside is varying, causing the change in capacitance $\Delta C(V_{TG})$. This expression describing ΔC can be simplified to $C_g^2/(C_g + C_q)$.

The resonance condition of an LC-circuit $f_{res} = 1/(2\pi\sqrt{LC(V_{TG})})$ can be expanded for small variations ΔC of the capacitance, yielding $\Delta C = -2(C_{cables} + C_g)\Delta f/f_0$. Applying this relation to the frequency data yields the curve displayed in figure 3(b). A minimum is visible at the charge neutrality point and an increase of ΔC with increasing density is observed. In this regime, the quantum capacitance dominates the signal. The transition to a constant capacitance value at large top-gate voltages indicates that C_q is negligible beyond ± 1 V.

Combining the two expressions for ΔC relates the quantum capacitance to the cable capacitance, the geometric capacitance and the measured frequency:

$$C_q = C_g \frac{\alpha - \delta_m}{\delta_m}, \quad (4)$$

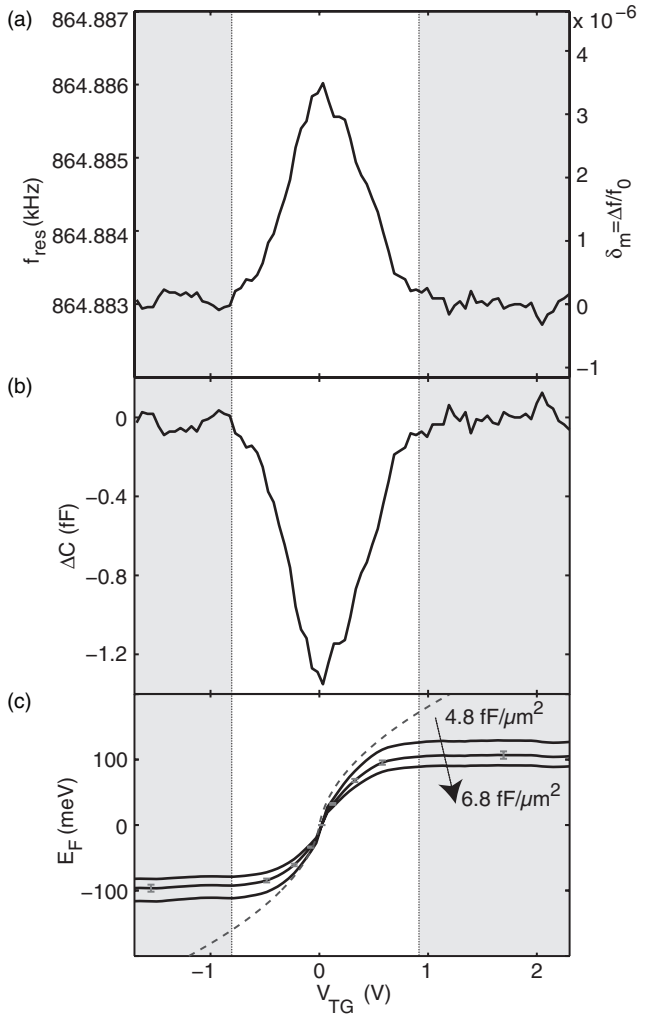

Figure 3. (a) Resonance frequency as a function of applied top-gate voltage V_{TG}. (b) Change in total capacitance determined from the frequency measurements in (a). (c) Relation between Fermi energy and top-gate voltage as deduced from equation (7). The different curves (black lines) are obtained for different values of C_g (from the outermost to the innermost curve: 4.8, 5.8 and 6.8 fF μm^{-2}). The dashed curve shows the theoretically expected dependence for a perfectly clean graphene sheet. To compensate for the shift of the Dirac point towards negative voltages, the horizontal axis in (a), (b) and (c) is offset by 0.3 V.

where $\alpha = C_g/2C_{cables}$. This equation contains only experimental parameters and will later be used to deduce the density of states $\mathcal{D}(E) = C_q(V_{TG})/|e|^2$.

In order to extract the density of states as a function of the Fermi energy, the top-gate voltage axis has to be transformed into energy. To avoid any *a priori* assumptions about the density of states, we do not use the linear dispersion but start with the electrostatic configuration described by equation (1). The charge carrier density n_s is obtained by integrating the density of states $\mathcal{D}(E)$ over all energies between the Dirac point and the Fermi energy E_F and can be substituted to give

$$|e|V_{TG} = E_F + \frac{|e|^2}{\epsilon\epsilon_0} d \int_0^{E_F} \mathcal{D}(E) \mathrm{d}E. \quad (5)$$

As shown above, both the geometric capacitance C_g and the quantum capacitance C_q enter this expression. The change in Fermi energy for a given change in top-gate voltage can hence

be written as

$$\frac{\partial E_F}{\partial V_{TG}} = |e| \left[1 + \frac{C_q(V_{TG})}{C_g} \right]^{-1}. \quad (6)$$

The relation between the capacitances involved and the measured frequency identified before can be included in equation (6). An expression for the Fermi energy which depends on the applied top-gate voltage is gained by integration over V_{TG}:

$$E_F(V_{TG}) = \frac{|e|}{\alpha} \int_{V_D}^{V_{TG}} \delta_m(V'_{TG}) dV'_{TG}, \quad (7)$$

where V_D is the gate voltage at the Dirac point. Here the geometric capacitance is the only parameter our device does not allow us to determine from the data directly. We can however estimate it from the parallel plate capacitor geometry (as has been done above to deduce the charge carrier mobility) to be $C_g \approx 6\,\mathrm{fF}\,\mu\mathrm{m}^{-2}$. In addition to the ribbon device, a bilayer Hall bar located on the same chip was used to determine the charge carrier density from Hall measurements. A geometric capacitance of $C_g \approx 5.8\,\mathrm{fF}\,\mu\mathrm{m}^{-2}$ was obtained by this method. Since the two values are comparable, the estimate for the free parameter C_g seems reasonable.

Equation (7) can now be applied to the data assuming a specific C_g. In figure 3(c), the obtained Fermi energy is plotted as a function of top-gate voltage for three different values of C_g as well as for an ideal graphene sheet (dashed curve). As expected, an increase of $|E_F|$ with increasing $|V_{TG}|$ is observed. This effect is strong at small voltages. The (unphysical) saturation at $|V_{TG}| > 1$ V indicated in figure 3 is due to the dominating cable capacitance. For all experimental curves, the Fermi energy at a certain top-gate voltage is below the theoretically expected value. As the noise in the frequency measurement leads to an error in the $E_F(V_{TG})$ relationship extracted from the measurement, an error analysis is done. The accuracy is estimated assuming a Gaussian probability density distribution for the relative frequency change $\Delta f/f_0$. Its width is given by the variance of the noise in δ_m, yielding $\sigma = 2.5 \times 10^{-7}$. The resulting error bars indicated in figure 3(c) are small in comparison to the uncertainty given by the parameter C_g.

Equations (4) and (7) now allow us to convert the data in figure 3(b) into a $\mathcal{D}(E_F)$ plot. The result is shown in figure 4 for different C_g values between 4.8 and 6.8 fF μm^{-2}. For comparison, the dashed line in figure 4 displays the theoretical density of states of perfectly clean graphene given by $\mathcal{D}(E_F) = 2E_F/\pi(v_F\hbar)^2$ [4]. In particular, at low energies a large discrepancy is observed between experiment and theory. Instead of the linear increase starting at zero, a nearly constant value of $\mathcal{D}(E_F) \approx 1 \times 10^{17}\,\mathrm{m}^{-2}\,\mathrm{eV}^{-1}$ is maintained in the interval between $E_F = \pm 50$ meV. An increase in the number of states towards higher energies is observed. However, since the signal to noise ratio decreases rapidly as the measurement value is constant at high charge carrier densities, the errors in the extracted $\mathcal{D}(E_F)$ become very large outside the interval limited by the grey areas in figure 4. The full width at half maximum of the probability density function of $\mathcal{D}(E_F)$ was used to determine the error bars shown in the graph.

The observed nonzero density of states around the charge neutrality point indicates a finite number of states. This is conceivable in the presence of local potential fluctuations in the graphene sheet. From the flat portion of the density of states in figure 4, we can estimate a characteristic amplitude of the fluctuations of 100 meV. Comparing our results with transport measurements on graphene nanoribbons [18–22] and scanning tunnelling electron transistor experiments [23], we find good agreement. As these samples were not covered with any dielectric unlike the sample used in our experiment, we can infer that the gate oxide did not induce a large amount of additional disorder in our graphene device.

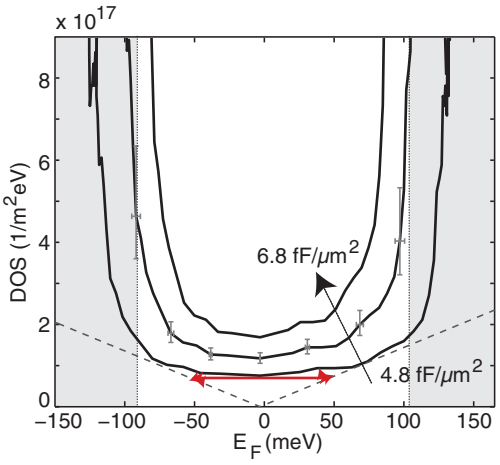

Figure 4. Density of states as a function of Fermi energy. The black solid lines show the experimental data assuming different C_g (from the outermost to the innermost curve: 4.8, 5.8 and 6.8 fF μm^{-2}). Error bars are indicated and the theoretically expected density of states for a perfectly clean graphene sheet is drawn as the dashed line. The bias window defined in figure 3 is plotted with dotted lines and the disorder amplitude is indicated by the red arrow.

6. Conclusions

We have performed transport and capacitance measurements on a locally gated single-layer graphene sheet. With our measurement setup, using a resonant circuit we could measure the capacitance with very high sensitivity. The density of states as a function of Fermi energy was determined from experimental data. As the main results, we extracted a constant density of states $\mathcal{D}(E_F) \approx 1 \times 10^{17}\,\mathrm{m}^{-2}\,\mathrm{eV}^{-1}$ around the Dirac point and determined the size of the disorder potential to be $\approx$100 meV, which is comparable to other studies.

It has recently been shown that the reduction of the disorder fluctuations (e.g. by using different substrates [24, 25]) improves the quantum capacitance signal dramatically and even allows for the investigation of Landau level formation in capacitance measurements [26–28].

References

[1] Smith T P, Goldber B B, Stiles P J and Heiblum M 1985 *Phys. Rev.* B **32** 2696
[2] Stern F 1983 *Appl. Phys. Lett.* **43** 974
[3] Ilani S, Donev L A K, Kindermann M and McEuen P L 2006 *Nature Phys.* **2** 687
[4] Wallace P R 1947 *Phys. Rev.* **71** 622

[5] Novoselov K S, Geim A K, Morozov S V, Jiang D, Katsnelson M I, Grigorieva I V, Dubonos S V and Firsov A A 2005 *Nature* **438** 197
[6] Tan Y-W, Zhang Y, Bolotin K, Zhao Y, Adam S, Hwang E H, Das Sarma S, Stormer H L and Kim P 2007 *Phys. Rev. Lett.* **99** 246803
[7] Fang T, Konar A, Xing H and Jena D 2007 *Appl. Phys. Lett.* **91** 092109
[8] Shylau A A, Klos J W and Zozoulenko I V 2009 *Phys. Rev.* B **80** 205402
[9] Chen Z and Appenzeller J 2008 *IEEE IEDM Tech. Digest* **21.1** 509
[10] Xia J, Chen F, Li J and Tao N 2009 *Nature Nanotechnol.* **4** 505
[11] Dröscher S, Roulleau P, Molitor F, Studerus P, Ensslin K and Ihn T 2010 *Appl. Phys. Lett.* **96** 152104
[12] Luryi S 1988 *Appl. Phys. Lett.* **52** 501
[13] Ihn T 2010 *Semiconductor Nanostructures* (Oxford: Oxford University Press)
[14] Davies J H 1998 *The Physics of Low Dimensional Semiconductors* (Cambridge: Cambridge University Press)
[15] Novoselov K S, Geim A K, Morozov S V, Jiang D, Zhang Y, Dubonos S V, Grigorieva I V and Firsov A A 2004 *Science* **306** 666
[16] Ferrari A C *et al* 2006 *Phys. Rev. Lett.* **97** 187401
[17] Graf D, Molitor F, Ensslin K, Stampfer C, Jungen A, Hierold C and Wirtz L 2007 *Nano Lett.* **7** 238
[18] Stampfer C, Güttinger J, Hellmüller S, Molitor F, Ensslin K and Ihn T 2009 *Phys. Rev. Lett.* **102** 056403
[19] Molitor F, Jacobsen A, Stampfer C, Güttinger J, Ihn T and Ensslin K 2009 *Phys. Rev.* B **79** 075426
[20] Todd K, Chou H T, Amasha A and Goldhaber-Gordon D 2009 *Nano Lett.* **9** 416
[21] Liu X, Oostinga J B, Morpurgo A F and Vandersypen L M K 2009 *Phys. Rev.* B **80** 121407
[22] Han M Y, Brant J C and Kim P 2009 *Phys. Rev. Lett.* **104** 056801
[23] Martin J, Akerman N, Ulbricht G, Lohmann T, Smet J H, Klitzing K V and Yacoby A 2008 *Nature Phys.* **4** 144
[24] Dean C R *et al* 2010 *Nature Nanotechnol.* **5** 77
[25] Xue J, Sanchez-Yamagishi J, Bulmash D, Jacquod P, Deshpande A, Watanabe K, Taniguchi T, Jarillo-Herrero P and LeRoy B J 2011 *Nature Mater.* **10** 282
[26] Young A F, Dean C R, Meric I, Sorgenfrei S, Ren H, Watanabe K, Taniguchi T, Hone J, Shepard K L and Kim P 2010 arXiv:1004.5556v2
[27] Ponomarenko L A, Yang R, Gorbachev R V, Blake P, Mayorov A S, Novoselov K S, Katsnelson M I and Geim A K 2010 *Phys. Rev. Lett.* **105** 136801
[28] Henriksen E A and Eisenstein J P 2010 *Phys. Rev.* B **82** 041412